Electronic Variations in Carbonate- and Phosphane-Related 24- and 26-Electron E_4 Clusters of Silicon and Germanium

Reinard Nesper,* Steffen Wengert, Fabio Zürcher, and Antonio Currao[a]

Abstract: The crystal structures and physical properties of four new Zintl compounds, $M_{5+x}Mg_{18-x}E_{13}$ (M = Sr, Ba; E = Si, Ge), are presented. The compounds are isotypic and crystallize with a novel structure type in *P*62*m*. The anionic sublattice is built of isolated E atoms and starlike E_4 clusters. The planar naked trisilylsilane Si_4 cluster anion was first discovered in the compound $Li_{12}Si_7$ and has given rise to many discussions. Temperature-dependent resistivity measurements show the compounds to be metallic, while measurements of the magnetic susceptibility indicate the presence of temperature-independent Pauli paramagnetism. The electronic structure of the compounds is investigated on the basis of ab initio band structure calculations and the results of the latter are in good agreement with the physical properties. The analysis of the electron localization function (ELF) proves to be a useful tool for gaining a better understanding of the present bonding situation.

Keywords: electron localization function · electronic structure · germanium · silicon · structure elucidation · Zintl phases

Introduction

The planar naked trisilylsilane Si_4 cluster anion was first discovered in 1980 in the compound $Li_{12}Si_7$;[1, 2] this compound gave rise to many discussions[3] because, despite its diamagnetism and its semiconducting behavior, chemical valence rules could not be applied in a straightforward way. The structure contains two different types of Zintl anions, according to the formulation $Li_{24}[Si_5]_2[Si_4]$. A molecular-like description of isolated silicon clusters did only allow for formulations of the electronic structure by paired (diamagnetism) and localized (semiconductor) electrons according to $(Li^+)_{24}[Si_5^{10-}]_2[Si_4^{4-}]$ (A), $(Li^+)_{24}[Si_5^{8-}]_2[Si_4^{8-}]$ (B), and $(Li^+)_{24}[Si_5^{6-}]_2[Si_4^{12-}]$ (C). However, open questions remained: the purely σ-bonded $[Si_5^{10-}]$ ion in (A) is not expected be planar, and a planar $[Si_5^{8-}]$ ion like in (B) should be a radical according to Hunds rules.

Shortly thereafter, on the basis of semiempirical INDO calculations (INDO = intermediate neglect of differential overlap) a description according to (C) was proposed,[4, 5] which, however, has the drawback that $[Si_4^{12-}]$ is isolectronic to ClF_3 but of different shape. Consequently, two electrons were assigned to the coordinating lithium shell around this cluster and localized in a so-called cage orbital.[6] Even then, the planarity of a $[Si_4^{10-}]$ ion was somewhat ackward. Some other Zintl phases with not really understood planar groups had already been reported at that time.[7, 8] Practically at the same time, the assumption of a quasi-aromatic pentasilapentadienyl group according to description (C) was supported by the compound Li_8MgSi_5,[9] which was consistently understood as $(Li^+)_3Mg^{2+}[Si_5^{6-}][Si^{4-}]$ on the basis of INDO calculations[5, 10] and its semiconducting and diamagnetic behavior. However, this compound does not contain the E_4 stars.[9]

Finally an ab initio localized-spherical-wave calculation on crystalline $Li_{12}Si_7$ by van Leuken et al.[11] provided new insights into the compound and supported a description similar to model (B) with a planar $[Si_4^{8-}]$ ion, which had first been suggested by Schnering et al.[2] The main difference to the latter was that in the picture generated by van Leuken et al. two electrons less reside in the Si_5 ring, while a Li atom in the neighborhood of this unit has its 2s shell filled, resulting in $[Li^+]_{22}[Li^-]_2[Si_5^{6-}]_2[Si_4^{8-}]$. While this interpretation in terms of $[Li^-]$ and $[Si_5^{6-}]$ gave rise to further questions and a renewed investigation,[12] the formulation of a $[Si_4^{8-}]$ ion seems to be quite reasonable. The novel ternary Zintl phases $M_{5+x}Mg_{18-x}E_{13}$ (M = Sr, Ba, E = Si, Ge), which are isotypic (although the strontium compounds have a slightly different ratio of earth alkaline metals), exclusively contain planar E_4 clusters and thus allow an independent test of the results of the recent calculation on $Li_{12}Si_7$.[12] On the basis of the chemical and structural data different valence electron counts are found for the starlike Si_4 and Ge_4 clusters in the new ternary compounds and the binary $Li_{12}Si_7$ which give rise to a new understanding of the internal redox capacity of such planar E_4 groups.

[a] Prof. Dr. R. Nesper, Dr. S. Wengert, Dr. F. Zürcher, Dr. A. Currao
Laboratorium für Anorganische Chemie
Eidgenössische Technische Hochschule Zürich (Switzerland)
Fax: (+41) 1-632-1149
E-mail: nesper@inorg.chem.ethz.ch

  0947-6539/99/0511-3382 $ 17.50+.50/0

Experimental Section

The compounds were synthesized from mixtures of the pure elements (Mg pieces (Fluka 99.8%), Sr pieces (ALFA 99%), Ba rods (ALFA 99.9%), Si powder (ALFA 99.99%), Ge lump (ALFA 99.9999%) which were sealed under an argon atmosphere in niobium ampoules and transferred into a furnace under vacuum. All compounds decomposed readily under contact with air and moisture. The phase purity of the samples was checked by X-ray diffraction (XRD) investigations on the powder, and thermal properties were studied by differential thermal analysis (DTA).

$Sr_{6.3}Mg_{16.7}Si_{13}$ (1): Compound **1** decomposes peritectically above 1380 K to give SrMgSi and a melt of Sr/Mg. Consequently, pure phase material was not yielded at stoichiometric amounts of the elements, even after annealing the mixture below the decomposition temperature. A maximum yield of crystalline $Sr_{6.3}Mg_{16.7}Si_{13}$ was gained by cooling a melt of the composition Sr:Mg:Si of 1:5:6 from 1570 K at 50 K per hour. The compound forms brittle silvery, platelike crystals of metallic luster.

$Ba_5Mg_{18}Si_{13}$ (2), $Sr_{6.3}Mg_{16.7}Ge_{13}$ (3), and $Ba_5Mg_{18}Ge_{13}$ (4): Compounds **2**–**4** melt congruently at 1370, 1400, and 1370 K, respectively. Pure phase samples of good crystallinity were gained from the melts by cooling. Neither in the system Sr/Mg/Si nor in the systems Sr/Mg/Ge was it possible to synthesize compounds of the stoichiometry $Sr_5Mg_{18}E_{13}$ (E = Si,Ge). Since the compounds **2**–**4** were synthesized in a fairly high purity (no extra lines in the X-ray pattern), an investigation of the physical properties, namely measurements of the conductivity and the magnetic susceptibility, appeared reasonable. The conductivity measurements were performed on pellets that had been pressed from powder samples (diameter 6 mm, thickness 1 mm, p 0.5 kbar). These were sintered under inert conditions at 1200 K for two days to reduce the influence of grain boundaries. A four-point van der Pauw method was applied after four gold contacts had been sputtered onto the pellets surface. In all three cases the temperature dependence of the resistance (Figure 1) shows metallic behavior with specific resistance of $\rho(0\,K) = 9.7 \times 10^{-5}$ Ωcm (**2**), $\rho(0\,K) = 6.0 \times 10^{-3}$ Ωcm (**3**), and $\rho(0\,K) = 2.2 \times 10^{-4}$ Ωcm (**4**). This is basically supported by the magnetic susceptibility measurements (Figure 1) which indicate temperature-independent (Pauli) paramagnetic behavior with $\chi_{mol} = 1.0 \times 10^{-3}\,cm^3mol^{-1}$ (**2**), $\chi_{mol} = 8.0 \times 10^{-3}\,cm^3mol^{-1}$ (**3**), and $\chi_{mol} = 2.1 \times 10^{-2}cm^3\,mol^{-1}$ for (**4**).

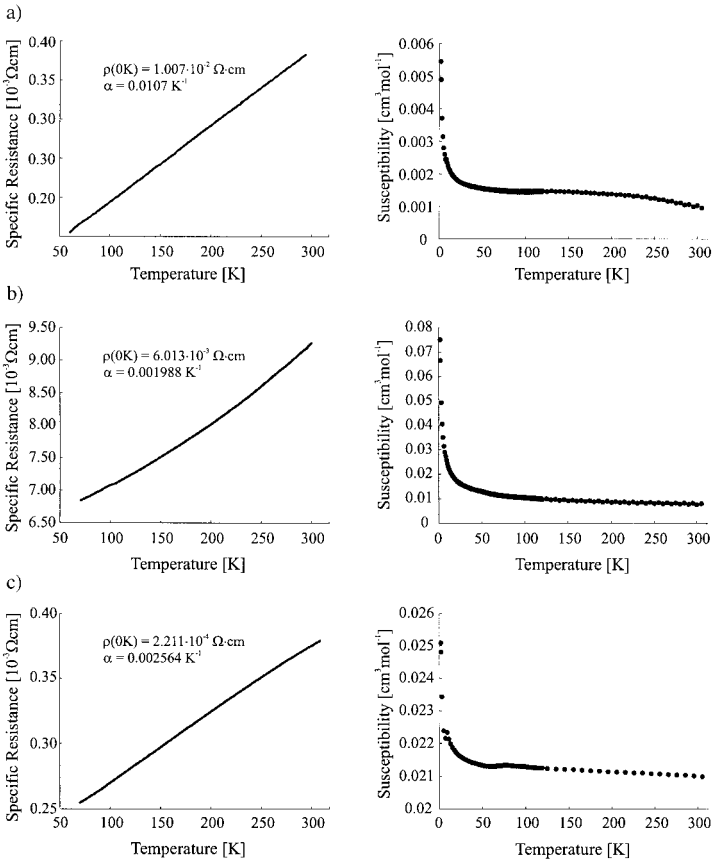

Figure 1. Temperature-dependent measurements of specfic resistance and magnetic susceptibility of $Ba_5Mg_{18}Si_{13}$ (a), $Sr_{6.3}Mg_{16.7}Ge_{13}$ (b), and $Ba_5Mg_{18}Ge_{13}$ (c).

Results and Discussion

Crystal structures

All presented crystal structures have been determined from single-crystal X-ray data. The compounds are isotypic and crystallize with a novel structure type. The Laue symmetry, 6/*mmm* and the lack of systematic extinctions confine the possible space groups to the symmorphic groups *P*622, *P*6*mm*, *P*$\bar{6}$2*m*, *P*$\bar{6}$*m*2, and *P*6/*mmm*. The structures were solved and refined in *P*$\bar{6}$2*m* and the quality of the structure determinations is good in all four cases.[13–16] The lattice constants and the atomic positions show only moderate deviations, which, on the one hand, in a very reasonable way express the size differences between Sr and Ba and on the other betweeen Si and Ge (Table 1 and Table 2).

Table 1. Lattice constants of the compounds $M_{5+x}Mg_{18-x}E_{13}$.

		a [Å]	c [Å]
$Sr_{6.3}Mg_{16.7}Si_{13}$ (**1**)	*P*$\bar{6}$2*m*	14.640(1)	4.4313(3)
$Ba_5Mg_{18}Si_{13}$ (**2**)	*P*$\bar{6}$2*m*	14.606(3)	4.4818(9)
$Sr_{6.3}Mg_{16.7}Ge_{13}$ (**3**)	*P*$\bar{6}$2*m*	14.711(1)	4.4459(2)
$Ba_5Mg_{18}Ge_{13}$ (**4**)	*P*$\bar{6}$2*m*	14.727(1)	4.5093(3)

Figure 2 shows a perspective view on the structure of $Ba_5Mg_{18}Si_{13}$ along [001] The silicon sublattice is built of a starlike Si_4 cluster and isolated silicon atoms. However, there are two peculiarities that should be discussed in more detail: the first is the mixed occupancy of one position (M(3), 3f) by Sr and Mg in $Sr_{6.3}Mg_{16.7}Si_{13}$ (**1**) and $Sr_{6.3}Mg_{16.7}Ge_{13}$ (**3**) which leads to a deviation in stoichiometry compared to the two barium compounds $Ba_5Mg_{18}Si_{13}$ (**2**) and $Ba_5Mg_{18}Ge_{13}$(**4**). The Wyckoff site 3f, which in the latter is completely occupied by Mg, is a somehow geometrically unusual position because it

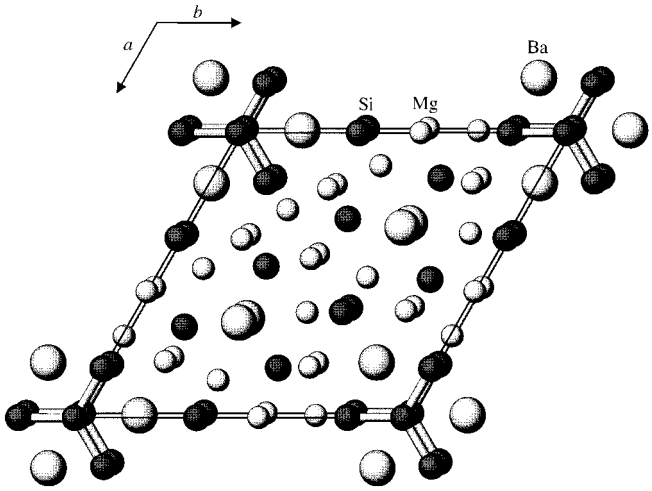

Figure 2. Perspective view on the structure of $Ba_5Mg_{18}Si_{13}$.

  0947-6539/99/0511-3383 $ 17.50+.50/0

Table 2. Wyckoff sites, atomic coordinates, and equivalent isotropic displacement parameters [pm^2] of the compounds $M_{5+x}Mg_{18-x}E_{13}$.

Atom	Wyckoff site	Compound		x	y	z	n_{occ}	U_{eq}
EA(1)	2c	(**1**)	Sr	1/3	2/3	0	1	170(2)
EA(1)	2c	(**2**)	Ba	1/3	2/3	0	1	147(3)
EA(1)	2c	(**3**)	Sr	1/3	2/3	0	1	173(4)
EA(1)	2c	(**4**)	Ba	1/3	2/3	0	1	177(2)
EA(2)	3g	(**1**)	Sr	0.81884(4)	0	1/2	1	181(2)
EA(2)	3g	(**2**)	Ba	0.81528(6)	0	1/2	1	149(3)
EA(2)	3g	(**3**)	Sr	0.17662(9)	0	1/2	1	196(3)
EA(2)	3g	(**4**)	Ba	0.18270(4)	0	1/2	1	183(2)
Mg(1)	3g	(**1**)	Mg	0.2768(2)	0	1/2	1	159(3)
Mg(1)	3g	(**2**)	Mg	0.2782(4)	0	1/2		136(11)
Mg(1)	3g	(**3**)	Mg	0.7217(4)	0	1/2	1	170(11)
Mg(1)	3g	(**4**)	Mg	0.7203(2)	0	1/2	1	171(6)
Mg(2)	6k	(**1**)	Mg	0.8754(2)	0.5187(2)	1/2	1	171(3)
Mg(2)	6k	(**2**)	Mg	0.8765(3)	0.5152(3)	1/2	1	177(8)
Mg(2)	6k	(**3**)	Mg	0.3574(3)	0.8767(3)	1/2	1	191(8)
Mg(2)	6k	(**4**)	Mg	0.3612(2)	0.8773(2)	1/2	1	191(4)
M(3)	3f	(**1**)	Mg/Sr	0.43860(6)	0	0	0.561(3)/0.439(3)	173(2)
M(3)	3f	(**2**)	Mg	0.4418(3)	0	0	1	206(10)
M(3)	3f	(**3**)	Mg/Sr	0.5601(2)	0	0	0.559(8)/0.441(8)	174(7)
M(3)	3f	(**4**)	Mg	0.5574(2)	0	0	1	296(8)
Mg(4)	6k	(**1**)	Mg	0.6267(2)	0.8056(2)	0	1	165(3)
Mg(4)	6k	(**2**)	Mg	0.6264(3)	0.8030(4)	0	1	162(10)
Mg(4)	6k	(**3**)	Mg	0.3737(3)	0.1945(3)	0	1	172(8)
Mg(4)	6k	(**4**)	Mg	0.3739(2)	0.1977(2)	0	1	182(4)
E(1)	1a	(**1**)	Si	0	0	0	1	391(9)
E(1)	1a	(**2**)	Si	0	0	0	1	530(40)
E(1)	2e	(**3**)	Ge	0	0	0.0990(2)	1/2	427(15)
E(1)	2e	(**4**)	Ge	0	0	0.0937(8)	1/2	383(8)
E(2)	3f	(**1**)	Si	0.1727(1)	0	0	1	165(3)
E(2)	3f	(**2**)	Si	0.1712(4)	0	0	1	161(12)
E(2)	3f	(**3**)	Ge	0.8278(2)	0	0	1	158(4)
E(2)	3f	(**4**)	Ge	0.18266(1)	0	0	1	161(2)
E(3)	3f	(**1**)	Si	0.6381(1)	0	0	1	153(3)
E(3)	3f	(**2**)	Si	0.6305(3)	0	0	1	167(10)
E(3)	3f	(**3**)	Ge	0.3609(2)	0	0	1	164(3)
E(3)	3f	(**4**)	Ge	0.3693(1)	0	0	1	161(2)
E(4)	6k	(**1**)	Si	0.8302(1)	0.3102(1)	1/2	1	150(2)
E(4)	6k	(**2**)	Si	0.8334(3)	0.3100(3)	1/2	1	159(7)
E(4)	6k	(**3**)	Ge	0.1698(1)	0.6893(1)	1/2	1	148(3)
E(4)	6k	(**4**)	Ge	0.1675(1)	0.6896(1)	1/2	1	169(2)

has only one close and four very far neighbors. In the strontium compounds there is a 45:55 Sr to Mg occupation of M(3). This results in one very short Sr–Si distance of 292 pm and in case of the germanium compound 293 pm, and four distances of usual length of 315 pm and 317 pm, respectively (Table 3). The shortest Sr–Si distances observed so far in related Zintl phases are 301 pm in $Sr_{13}Mg_2Si_{20}$,[17] 302 pm in $Sr_2Mg_{2-x}Si_3$ ($x = 0.38$),[18] and 308 pm in $SrMgSi_2$.[19] On the basis of effective coordination numbers (ECON[20]) and bond length bond strength considerations the distance of 292 pm is tolerable but unusual. On the basis of the sums of radii an effective radius of at least 180 pm is calculated for the terminal silicon atom and one of 109 pm for the Sr^{2+} ion with a coordination number five, which yields a Sr–Si distance of 289 pm. Thus, radii are difficult to apply since it is known that negatively charged silicon species are extremely polarizable. The chemical analysis of a pure phase sample of $Sr_{6.3}Mg_{16.7}Ge_{13}$ did not give any indication for a calcium content in this compound that

Table 3. Atomic distances (esd) [pm] for $Sr_{6.3}Mg_{16.7}Si_{13}$ n denotes the frequency of the corresponding distances.

Atom pair	d	n	Atom pair	d	n	Atom pair	d	n
Sr1 –Si4	340.14(7)	6	Mg2–Mg2	315.8(3)		Mg4–Sr1	372.06(13)	
Sr1–Mg2	364.96(11)	6	Mg2–Mg4	317.36(14)	2			
Sr1–Mg4	372.06(13)	3	Mg2–M3	342.73(12)	2	Si1–Si2	252.9(2)	3
			Mg2–Sr1	364.96(11)	2	Sr1–Sr2	345.58(4)	6
Sr2–Si2	341.03(6)	4	Mg2–Sr2	382.4(2)				
Sr2–Si3	345.14(12)	2				Si2–Si1	252.9(2)	
Sr2–Si1	345.58(4)	2	M3–Si3	292.0(2)		Si2–Mg1	268.9(2)	
Sr2–Mg1	356.5(2)	2	M3–Si4	315.41(8)	4	Si2–Mg4	279.2(2)	2
Sr2–Mg4	359.44(12)	4	M3–Mg4	320.5(2)	2	Si2–Sr2	341.03(6)	4
Sr2–Mg2	382.4(2)	2	M3–Mg1	324.3(2)	2			
			M3–Mg2	342.72(12)	4	Si3–Mg4	276.7(2)	2
Mg1–Si2	268.9(2)	2	M3–Si2	389.24(18)		Si3–Mg2	284.65(10)	4
Mg1–Si4	276.2(2)	2				Si3–Sr2	345.14(12)	
Mg1–Mg4	317.25(10)	4	Mg4–Si4	275.16(12)	2			
Mg1–M3	324.3(2)	2	Mg4–Si3s	276.7(2)		Si4–Mg2	272.7(2)	
Mg1–Sr2	356.5(2)	2	Mg4–Si2	279.2(2)		Si4–Mg4	275.15(12)	2
			Mg4–Mg1	317.24(10)	2	Si4–Mg1	276.2(2)	
Mg2–Si4	272.7(2)		Mg4–Mg2	317.36(14)	2	Si4–M3	315.41(8)	2
Mg2–Si4	278.1(2)		Mg4–M3	320.5(2)		Si4–Sr1	340.14(7)	2
Mg2–Si3	284.65(10)	2	Mg4–Sr2	359.43(12)	2			

0947-6539/99/0511-3384 $ 17.50+.50/0 *Chem. Eur. J.* **1999**, *5*, No. 11

might have explained the observed electron density on site 3f, as well. If the 3f site is occupied by magnesium the contacts yield a different meaning: the distance of 292 pm is medium-sized compared to Mg–Si and Mg–Ge distances which start from about 270 pm as observed for numerous silicides and germanides.[12, 21] The longer contacts, however, may somehow be considered as unfavorable for the small Mg^{2+} ion. This situation changes slightly in the barium compounds where the short contacts decrease to 276 and 277 pm, while the four other silicon and germanium neighbors are even further away (Table 4). In $Ba_5Mg_{18}Si_{13}$ and $Ba_5Mg_{18}Ge_{13}$ the displacement ellipsoid of M(3) shows the large positional freedom of this site quite well.[14, 16] In $Sr_{6.3}Mg_{16.7}Si_{13}$ and $Sr_{6.3}Mg_{16.7}Ge_{13}$ there is no special displacement of this position because the main scatterer Sr is supposed to be essentially fixed. However, the close neighbor Si(3) exhibits some elongation of the probability ellipsoid along this interatomic vector. In conclusion, the comparison of all four compounds supports our structure model that contains one fairly strained metal site in this structure type, which under certain circumstances may lead to a mixed occupation.

Table 4. Interatomic distances (esd) [pm] for $Ba_5Mg_{18}Si_{13}$ *n* denotes the frequency of the corresponding distances.

Atom pair	*d*	*n*	Atom pair	*d*	*n*	Atom pair	*d*	*n*
Ba1–Si4	344.9(3)	6	Mg2–Mg2	312.5(8)		Mg4–Ba1	370.9(4)	
Ba1–Mg2	365.1(3)	6	Mg2–Mg4	324.8(4)	2			
Ba1–Mg4	370.9(4)	3	Mg2–Mg3	337.1(4)	2	Si1–Si2	250.1(6)	3
			Mg2–Ba1	365.1(3)	2	Si1–Ba2	350.73(8)	6
Ba2–Si2	343.6(2)	4	Mg2–Ba2	381.5(4)				
Ba2–Si1	350.73(8)	2				Si2–Si1	250.1(6)	
Ba2–Si3	350.8(3)	2	Mg3–Si3	275.6(7)		Si2–Mg1	273.2(5)	
Ba2–Mg1	358.1(4)	2	Mg3–Si4	315.6(3)	4	Si2–Mg4	278.7(6)	2
Ba2–Mg4	360.2(4)	4	Mg3–Mg4	319.5(6)	2	Si2–Ba2	343.6(2)	4
Ba2–Mg2	381.5(4)	2	Mg3–Mg1	327.5(5)	2			
			Mg3–Mg2	337.1(4)	4	Si3–Mg2	284.1(3)	4
Mg1–Si4	269.6(5)	2	Mg3–Si2	395.1(8)		Si3–Mg4	284.8(5)	2
Mg1–Si2	273.2(5)	2				Si3–Ba2	350.8(3)	
Mg1–Mg4	316.6(3)	4	Mg4–Si4	274.3(4)	2			
Mg1–Mg3	327.5(5)	2	Mg4–Si2	278.7(6)		Si4–Mg1	269.6(5)	
Mg1–Ba2	358.1(4)	2	Mg4–Si3	284.8(5)		Si4–Mg4	274.3(4)	2
			Mg4–Mg1	316.6(3)	2	Si4–Mg2	278.6(6)	
Mg2–Si4	273.7(6)		Mg4–Mg3	319.5(6)		Si4–Mg3	315.6(3)	2
Mg2–Si4	278.6(6)		Mg4–Mg2	324.8(4)	2	Si4–Ba1	344.9(3)	2
Mg2–Si3	284.1(3)	2	Mg4–Ba2	360.2(4)	2			

The second peculiarity is found at the central atom Si1 and Ge1 of the E_4 star. This site shows a very pronounced anisotropic displacement for both of the two silicides (see Figure 4a), while in the germanides a slightly pyramidal Ge_4 group is resolved. These differences in the geometry of the E_4 star are reflected in the electron density distributions which can be calculated from the X-ray diffraction data. Figure 3 compares the electron density distribution of the barium compounds **2** and **4** in sections perpendicular to the plane of the star.

While the electron density map of the silicide **2** (Figure 3 top) shows only a strongly anisotropic distribution corresponding to the Si1 position, the map of the germanide (Figure 3 bottom) exhibits two distinct density maxima for the Ge1 position. Therefore, we refined the structures of the two

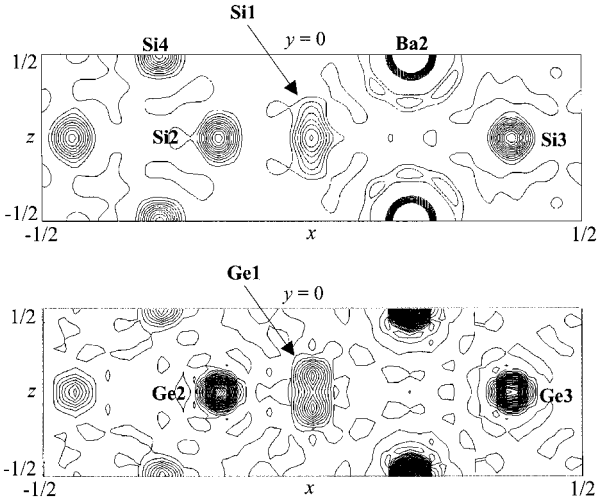

Figure 3. Electron density distributions of $Ba_5Mg_{18}Si_{13}$ (top) and $Ba_5Mg_{18}Ge_{13}$ (bottom) in sections perpendicular to the plane of the X_4 star.

germanides **3** and **4** by splitting the central atom of the star (0,0,0) into two positions (0,0,*z*).[15, 16] The mean displacements of the central silicon atoms Si1 from the mean plane of the clusters amount to 28(5) pm in **1** and 34(10) pm in **2** at room temperature. This compares fairly well with the displacement of the central germanium atom Ge1 in **3** of 42(1) pm and 50(6) in **4**.

In order to check whether an ordering of the pyramidal Si_4 cluster could be seen at lower temperatures measurements were taken at 170 K on a crystal of **2**.[22] These revealed that this is clearly not the case: while all displacement parameters are reduced by about 55 % the U_{33} term of Si1 only reduces by 17 %, which leaves the reduction still in the range of the standard deviation (Figure 4b). Consequently, it has to be

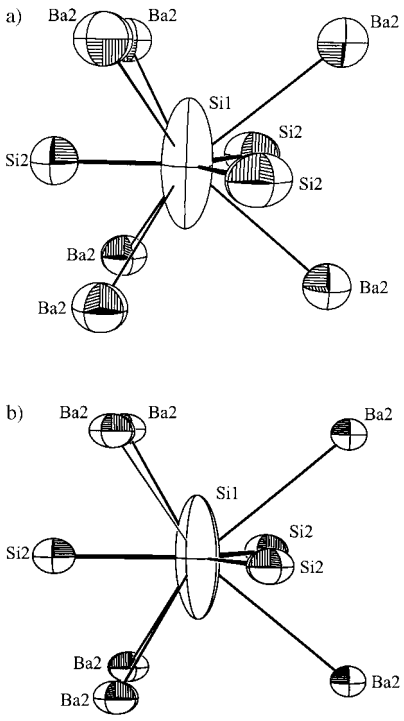

Figure 4. Coordination sphere of the starlike Si_4 unit in $Ba_5Mg_{18}Si_{13}$. Anisotropic displacements at room temperature (a), and at 170 K (b).

assumed that this displacement is mostly due to a static disorder of pyramidal Si_4 groups.

For all four compounds the electron count based on the observed compositions leaves a formal charge of $q = -10$ on the starlike units and thus makes them isoelectronic to the pyramidal EX_3 groups such as PCl_3. The assumption of a formal charge transfer in semiconductor compounds goes back to the so-called Zintl–Klemm concept[23–26] for semiconductors which actually does not really refer to charges but to the assignment of occupied electronic states to different atoms.[27] The formulation $(M^{2+})_{5+x}(Mg^{2+})_{18-x}(E_4{}^{10-})(E^{4-})_9$ (M = Sr, Ba; E = Si, Ge) then states that all occupied valence states have to be assigned to or, in other words, are to be localized at the E atoms.

Theoretical investigations

In order to check whether the simple assumptions of the Zintl–Klemm concept still hold for $Ba_5Mg_{18}Si_{13}$ (**2**) and $Ba_5Mg_{18}Ge_{13}$ (**4**), the electronic structures were investigated by using extended Hückel (EH[28]) and LMTO (linear muffin tin orbital) methods.[29] A first impression of the present bonding situation can be gained by an analysis of the electron localization function (ELF) calculated on the basis of the electronic wavefunction.[30, 31] In Figure 5 some structural sections are shown for which the ELF has been calculated (here, based on the LMTO method, the results using the EH method are comparable).

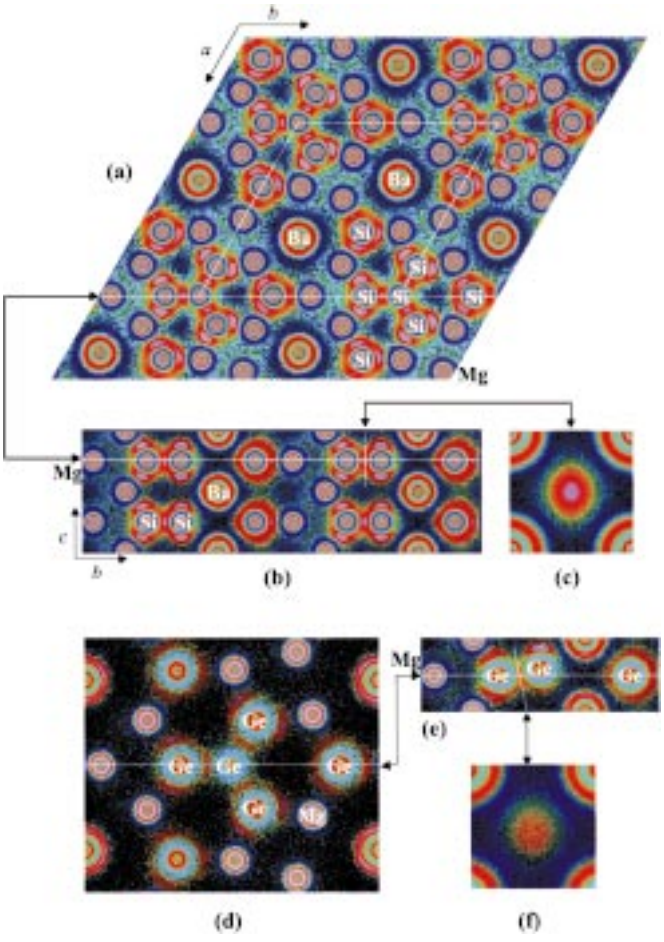

Figure 5. ELF distributions of $Ba_5Mg_{18}Si_{13}$ (**2**) and $Ba_5Mg_{18}Ge_{13}$ (**4**) in some structural sections. a) principal plane of X_4 unit in **2**; b) section perpendicular to principal plane of X_4 unit in **2**; c) Si–Si bond section; d) principal plane of X_4 unit in **4;** e) section perpendicular to principal plane of X_4 unit in **4**; Ge–Ge bond section. See text for details.

The principal plane of the X_4 units of **2** and **4** is shown in Figure 5a and 5d. The semimetal atoms Si and Ge are easily detected because of their nonspherical distribution pattern. In the light colored region (white, orange) electrons are highly localized, and these regions are interpreted in terms of atomic cores, chemical bonds, and lone pairs of electrons.[31] It is quite interesting to note how the lone pair shells at the isolated Si^{4-} ions are polarized towards the Mg^{2+} ions and away from the Ba^{2+} ions. The strongly localizing influence of the Mg^{2+} ion is also visible at the X_4 units in both displays. This illustrates the well-established strong interaction of Mg^{2+} with Zintl anions.[12] Both cation types appear just as cores with nearly spherical distributions and have no direct contact to the extended valence electron localization around silicon and germanium. Thus, the ELF distributions support quite directly the Zintl–Klemm approach, stating that all valence electrons are in states which exclusively have to be assigned to the semimetal atoms.[23–26]

The overall differences are smaller for the germanide: This is in agreement with the general trend that more electron-rich atoms especially those with occupied d and f states generate less pronounced ELF patterns. The low ELF around Ge1 in Figure 5d is due to the pyramidal geometry which shifts Ge1 out of the plane of the other three Ge atoms. The sections perpendicular to the principal plane of the X_4 groups show a well expressed p-shaped lone pair at the central Si1 atom for **2** (Figure 5b) and a more sp^3-shaped lone pair at the pyramidal Ge1 atom for **4** (Figure 5e). Clearly, this is different for a carbonate-like 24-electron system such as in $Li_{12}Si_7$, in which no lone pair localization at the central silicon atom is found.[12] The bond sections (Figure 5c and f) show a very small elliptical character which may be due to π contributions but also to polarization effects. The overall bonding characteristic is of σ-type.

A more detailed picture of the electronic situation can be obtained from an analysis of the electronic band structures. Figure 6a shows a LMTO band structure plot of $Ba_5Mg_{18}Si_{13}$ together with the corresponding electronic density of states (DOS). Clearly, there is no band gap at the Fermi level (E_F). Thus, the compound is supposed to show metallic properties, which is indeed supported by the results of the conductivity and magnetic susceptibility measurements.

At first these results were quite puzzling since they were in contrast to the outcome of the EH calculations which show significant band gaps, even after a charge iteration procedure. Here, the number and character of the occupied states were totally in agreement with the ideas of the Zintl–Klemm concept. As can be shown, this dilemma is due to an improper choice of the Slater exponents for the 3s and 3p basis functions of silicon ($\xi_{3s} = 1.383$, $\xi_{3p} = 1.383$[32]) for the EH calculations. Compared with the LMTO band structure the Si-s bands show larger and the Si-p bands smaller dispersions, respectively. This is very often found in calculations on Zintl phases of silicon[12] and points to the fact that the 3s function of silicon has to be contracted, while the 3p functions should be slightly more diffuse. Using a rough estimate of $\xi_{3s} = 1.9$ and $\xi_{3p} =$

0947-6539/99/0511-3386 $ 17.50+.50/0 *Chem. Eur. J.* **1999**, *5*, No. 11

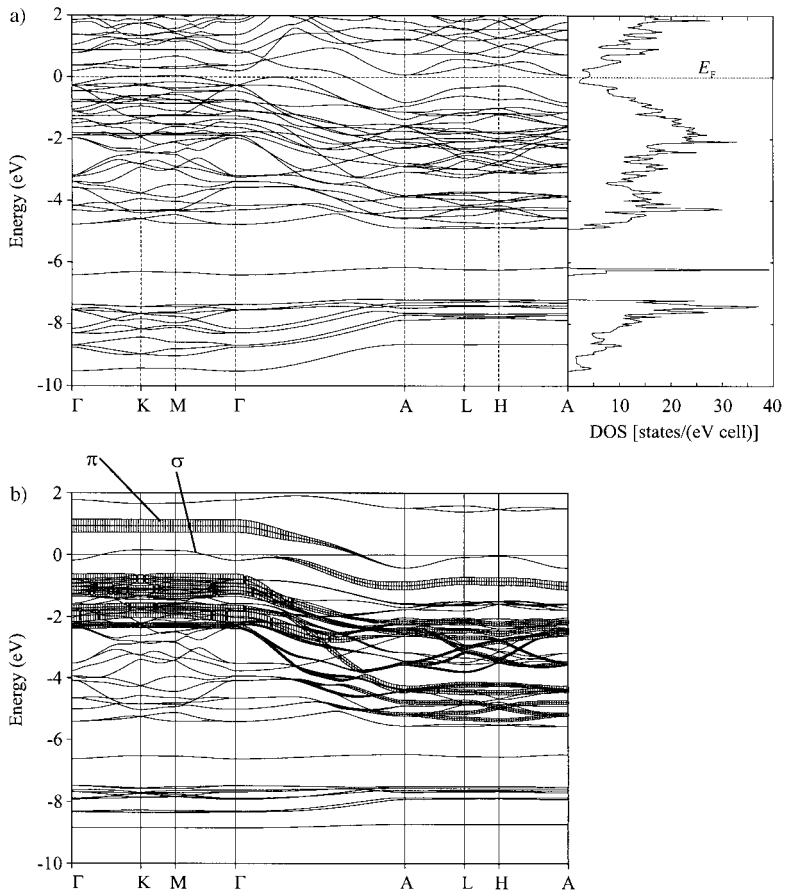

Figure 6. Electronic band structure and density of states of $Ba_5Mg_{18}Si_{13}$ (a), band structure of $Ba_5Mg_{18}Si_{13}$ with all metallic partial waves down-folded, the contributions of Si-p_z are figured out by *fatbands* (b).

1.2[33] for the basis functions of silicon, and performing a charge iteration with respect to the H_{ii} we end up with a band structure quite similar to that found in the LMTO–ASA calculation, especially in the energy region below and around E_F. The main effect of enlarging ξ_{3s} is a lowering of the antibonding σ^* levels of the Si_4 cluster (Figure 7). Together with a stabilization by the coordinating cations, especially barium, this leads to a band mainly due to the σ_{10} state competing with the highest π band, which is mainly due to the π_4 state close to E_F. In the case of an isolated Si_4^{10-} cluster we find partial π bonding at the expense of a slight weakening of the σ bonds.

To gain information in support of this interpretation we performed a LMTO–ASA calculation on $Ba_5Mg_{18}Si_{13}$ with the Ba-6s, Ba-6p, Mg-3s, and Mg-3p functions down-folded in the tails of the MTOs.[29] Thus we have only Si-3s and Si-3p MTOs in the basis set for the band structure calculation. The resulting band structure shown in Figure 6b is below and around E_F quite similar to that found in the full calculation (Figure 6a). The contribution of the Si-p_z function to the bands is determined by employing a *fatband analysis*.[29] Here, the broadening of a line is a measure of the corresponding Si-p_z contribution to that band. First, we can recognize the strong dispersion of the π bands along Γ→A due to their interaction along the stacking direction *c*. One has to keep in mind that from symmetric arguments a strict $\sigma-\pi$ separation is defined only in regions of the Brouillin zone with $\mathbf{k}=(x,y,0)$. If one concentrates on the region round E_F one may identify at Γ a degenerate band at about 2 eV based on the highest antibonding $\sigma_{11}\sigma_{12}$ orbitals, at about 1 eV a π band which is due to the highest antibonding π_4 orbital, and slightly below E_F the σ band based on the antibonding σ_{10} orbital of the Si_4 unit. Thus, compared with the isolated cluster there is an exchange between π_4 and σ_{10} of which the latter is occupied at Γ. This situation remains for all $\boldsymbol{k}=(x,y,0)$ (Γ, K, M). Things change totally if one focuses on regions with $\boldsymbol{k}=(x,y,1/2)$ (A, L, H). Here, the π_4 band lies below the σ_{10} band, as expected. Both bands are below E_F and thus occupied. Along the Γ→A direction there is an avoided crossing between the σ_{10} and the π_4 band leading to a change in the character of the bands.[*] So far, we are able to understand the band structure of $Ba_5Mg_{18}Si_{13}$ in terms of only silicon states, which strongly

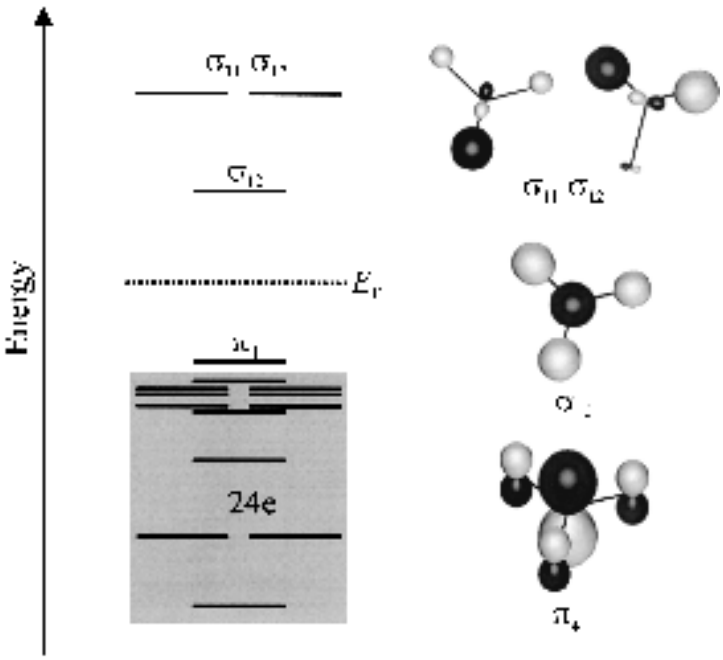

Figure 7. Scheme of the MO levels of an isolated Si_4^{10-} unit.

[*] This is due to the fact that in this region of the Brouillin zone both bands are of the same symmetry and thus cannot cross.

supports the Zintl–Klemm picture we used in our discussion, despite the fact that the compound displays metallic behavior.

The band structure of $Ba_5Mg_{18}Ge_{13}$ is not shown here. One finds nearly the same situation as in the silicon compound, even if the Ge_4 unit is slightly pyramidal. Again, $Ba_5Mg_{18}Si_{13}$ shows metallic behavior.

One important point of interest which we still have to settle is the question of planarity of the E_4 cluster. As was shown before, one can formally assume E_4^{10-} ions. A comparison of data for related units such as $Si(SiH_3)_3^-$ (d(Si–Si) = 2.379 Å, $\sphericalangle$(Si-Si-Si) = 98.6°[34]), and P_4^{6-} in Ni_5P_4 (d(P–P) = 2.19 Å, $\sphericalangle$(P-P-P) = 111.5°[35]) reveals that the planar situation is quite unfavorable for the 26-electron case. The structural results on the compounds **1**–**4** (pronounced anisotropic displacement or even split positions of the central atoms of the starlike E_4 unit) support this as well. A first step to study this problem in more detail is to perform geometry optimizations with respect to the position of the central atom of the E_4 cluster. From the previous static band structure investigations on $Ba_5Mg_{18}Si_{13}$ and $Ba_5Mg_{18}Ge_{13}$ it is clear that the geometry of the E_4 unit is strongly correlated with a subtle balance between the antibonding σ_{10} and π_4 levels.

The LMTO method in its atomic sphere approximation (ASA) used so far is known to be not suitable for such geometry optimization studies.[36] Thus, the investigations were restricted to more qualitative EH calculations. Due to a lack of repulsion terms in the simple EH method the optimization of distance dependencies is expected to give nonsensical results, but the study of angle dependencies is shown to be quite useful for a qualitative understanding of molecular geometry.[37, 38]

Figure 8 shows a Walsh diagram for $Ba_5Mg_{18}Si_{13}$ (based on the optimized Hückel parameters), which illustrates the change in total energy with respect to an out-of-plane displacement of the central Si1 atom of the Si_4 star. The pyramidal geometry is calculated to be significantly more stable. One finds an energy minimum for a displacement of the central Si1 atom of about 1.1 Å. The results are strongly dependent on the choice of the Slater exponents for silicon. In case of the standard parameters ($\xi_{3s} = 1.383$, $\xi_{3p} = 1.383$[32]) the minimum is shifted towards a value of 0.7 Å. It is clear that these EH considerations have only preliminary character. Ab initio studies based on Hartree Fock (HF) and FLAPW methods are topics of current investigations. These would burst the frame of the present work and will be reported later. However, the first results of the HF calculations[39] on $Ba_5Mg_{18}Si_{13}$ support these EH results. With an energy minimum for an out-of-plane displacement of 0.45 Å they show that the EH approach clearly overestimates the effects. Even the latter value seems to be slightly too large. Considering the large thermal displacement component of Si1 found in the structure refinement one would expect an elongation of about $\sqrt{U_{33}} = 0.32$ Å.

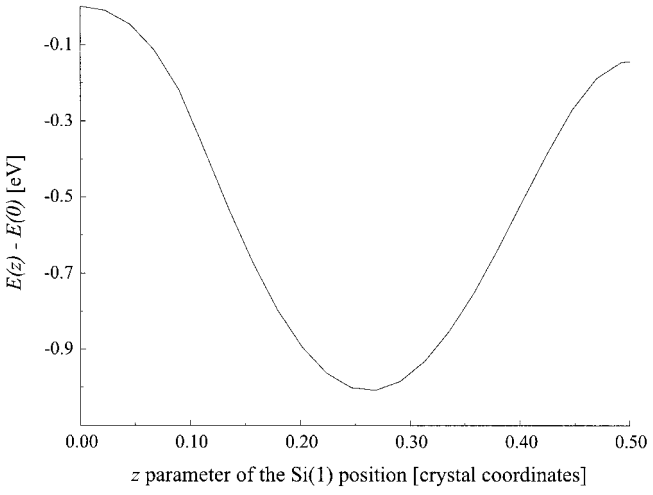

Figure 8. Walsh diagram for $Ba_5Mg_{18}Si_{13}$.

Conclusion

Considering our recent investigations on $Li_{12}Si_7$[12] the present work strongly supports that the starlike E_4 group may occur as a completely planar E_4^{8-} ion, which is isostructural and isoelectronic to CO_3^{2-}, or as an E_4^{10-} ion, which is slightly pyramidal and isoelectronic to PCl_3, for example. The pyramidality is expressed by the extraordinary anisotropic displacements for the silicides and by split positions in case of the germanides. The metallic behavior of the compounds is well understood with respect to their electronic band structures.

There are several interconnected reasons for the different redox states of the E_4 cluster, of which the stoichiometry is a trivial one but only if there is no competition between different electron reservoirs. Thus, it must be emphasized that not all cations are able to stabilize highly charged Zintl anions. For example, the Group 14 elements form the limiting E^{4-} ion only by coulomb stabilization of at least divalent cations. Except lithium, the monovalent alkali metal ions do not stabilize Group 14 elements to a higher formal charge than $q = -1$. Besides such cation–anion charge transfer relations, there may be competition between different Zintl anions for the electrons. The Zintl anions themselves change their electron uptake capacity with respect to their actual cation coordination as can be seen in case of the E_4 units.

Acknowledgment

We would like to thank C. Mensing for the conductivity measurements and the Swiss National Science Foundation for generous support under project no. 20–50675.97.

[1] H.-G. von Schnering, R. Nesper, K.-F. Tebbe, J. Curda, *Z. Metallkde.* **1980**, *71*, 357.
[2] H.-G. von Schnering, R. Nesper, J. Curda, K.-F. Tebbe, *Angew. Chem.* **1980**, *92*, 1070; *Angew. Chem. Int. Ed. Engl.* **1980**, *19*, 1033.
[3] J. Liebmann, J. Vincent, *Angew. Chem.* **1982**, *94*, 649; *Angew. Chem. Int. Ed. Engl.* **1982**, *21*, 632.
[4] M. C. Böhm, R. Ramírez, R. Nesper, H.-G. von Schnering, *Phys. Rev. B* **1984**, *30*, 4870.
[5] R. Ramírez, PhD thesis, Universität Stuttgart, **1986**.
[6] R. Ramírez, R. Nesper, H.-G. von Schnering, M. Böhm, *Z. Naturforsch. A* **1986**, *41*, 1267.
[7] W. Müller, H. Schäfer, A. Weiß, *Z. Naturforsch. B* **1970**, *25*, 1371.

  0947-6539/99/0511-3388 $ 17.50+.50/0 *Chem. Eur. J.* **1999**, *5*, No. 11

[8] W. Müller, H. Schäfer, A. Weiß, *Z. Naturforsch. B* **1971**, *26*, 5.
[9] R. Nesper, J. Curda, H.-G. von Schnering, *J. Solid State Chem.* **1986**, *170*, 199.
[10] R. Ramírez, R. Nesper, H.-G. von Schnering, M. Böhm, *Chem. Phys.* **1985**, *95*, 17.
[11] H. van Leuken, G. A. de Wijs, W. van der Lugt, R. A. de Groot, *Phys. Rev. B* **1996**, *53*, 10599.
[12] S. Wengert, PhD thesis no. 12070, ETH Zürich, **1997**.
[13] a) $Sr_{6.3}Mg_{16.7}Si_{13}$ (**1**): data collection: four-circle diffractometer (STADI4, STOE); $Mo_{K\alpha}$ radiation, full-matrix least-squares refinement of F^2,[40] range for data collection: $3.2^\circ < 2\Theta < 59.8^\circ$; $-20 < h < 20$, $-20 < k < 20$, $-6 < l < 6$; $R_{int} = 0.05$, $R_1 = 0.03$, $wR_2 = 0.06$ (all 958 independent reflections). b) Further details of the crystal structure investigations may be obtained from Fachinformationszentrum Karlsruhe, D-76344 Eggenstein-Leopoldshafen (Fax: (+49) 7247-808-666; e-mail: crysdata@fiz-karlsruhe.de), on quoting the depository numbers CSD-410453 (**1**), CSD-410450 (**2**), CSD-410452 (**3**), CSD-410449 (**4**), and CSD-410451 ($Ba_5Mg_{18}Si_{13}$ at $T = 173$ K).
[14] $Ba_5Mg_{18}Si_{13}$ (**2**): data collection: image plate diffractometer (IPDS, STOE); $Mo_{K\alpha}$ radiation, full-matrix least-squares refinement of F^2,[40] range for data collection: $8.5^\circ < 2\Theta < 48.2^\circ$; $-16 < h < 16$, $-16 < k < 16$, $-5 < l < 5$, $R_{int} = 0.05$, $R_1 = 0.03$, $wR_2 = 0.09$ (all 540 independent reflections).[13b]
[15] $Sr_{6.3}Mg_{16.7}Ge_{13}$ (**3**): data collection: four-circle diffractometer (STADI4, STOE); $Mo_{K\alpha}$ radiation, range for data collection: $3.2^\circ < 2\Theta < 59.8^\circ$; $-20 < h < 20$, $-20 < k < 20$, $-6 < l < 6$, full-matrix least-squares refinement of F^2,[40] $R_{int} = 0.13$, $R_1 = 0.06$, $wR_2 = 0.06$ (all 967 independent reflections). The structure was refined as an inversion twin (absolute structure parameter 0.34).[13b]
[16] $Ba_5Mg_{18}Ge_{13}$ (**4**): data collection: four-circle diffractometer (STADI4, STOE); $Mo_{K\alpha}$ radiation, full-matrix least-squares refinement of F^2,[40] range for data collection: $3.2^o < 2\Theta < 59.8^\circ$; $-20 < h < 20$, $-20 < k < 20$, $-6 < l < 6$, $R_{int} = 0.05$, $R_1 = 0.02$, $wR_2 = 0.06$ (all 981 independent reflections). The structure was refined as inversion twin (absolute structure parameter 0.57).[13b]
[17] A. Currao, R. Nesper, *Angew. Chem.* **1998**, *110*, 843; *Angew. Chem. Int. Ed.* **1998**,*37*, 841.
[18] A. Currao, PhD thesis no. 11747, ETH Zürich, **1996**.
[19] A. Currao, J. Curda, R. Nesper, *Z. Anorg. Allg. Chem.* **1996**, *622*, 85.
[20] R. Hoppe, *Angew. Chem.* **1966**, *78*, 52; *Angew. Chem. Int. Ed. Engl.* **1966**,*5*, 95.
[21] F. Zürcher, PhD thesis no. 12546, ETH Zürich, **1998**.
[22] $Ba_5Mg_{18}Si_{13}$: $P\bar{6}2m$; $T = 173$ K; $a = 14.571(3)$ and $c = 4.4667(9)$ Å. Data collection: image plate diffractometer (IPDS, STOE); $Mo_{K\alpha}$ radiation, full-matrix least-squares refinement of F^2.[40] Ba(1): 1/3, 2/3, 0, 0.0071(3); Ba(2): 0.81535(4), 0, 0.5, 0.0084(10); Mg(1): 0.2789(3), 0, 0.5, 0.0084(10); Mg(2): 0.8771(2), 0.5156(2), 0.5, 0.0093(7); Mg(3): 0.4420(3)), 0, 0, 0.0106(8); Mg(4): 0.6258(3), 0.8024(3), 0, 0.0073(8); Si(1): 0, 0, 0, 0.041(3); Si(2): 0.1718(3), 0, 0, 0.0096(11); Si(3): 0.6305(3), 0, 0, 0.0079(8); Si(4): 0.83023(8), 0.31017(9), 0.5, 0.0082(6); range for data collection: $8.5^\circ < 2\Theta < 48.0^\circ$; $-16 < h < 14$, $-16 < k < 16$, $-5 < l < 5$, $R_{int} = 0.10$, $R_1 = 0.02$, $wR_2 = 0.05$ (all 524 independent reflections).[13b]
[23] E. Mooser, W. B. Pearson, *Progress in Semiconductors*, *Vol. 5*, Wiley, New York, **1960**.
[24] W. Klemm, *Festkörperprobleme, Bd.III*, Vieweg, Braunschweig **1963**.
[25] E. Busmann, *Z. Anorg. Allg. Chem.* **1961**, *313*, 90.
[26] W. Klemm, E. Busmann, *Z. Anorg. Allg. Chem.* **1963**, *319*, 297.
[27] R. Nesper, *Prog. Solid State Chem.* **1990**, *20*, 1.
[28] U. Häußermann, R. Nesper, S. Wengert, T. F. Fässler; Program MEHMACC: modified Extended-Hückel version based on the QCPE programm EHMACC,[41] ETH Zürich, **1993**.
[29] G. Krier, O. Jepsen, A. Burkhardt, O. K. Andersen, TB–LMTO–ASA Program, Stuttgart, Germany, **1994**.
[30] A. D. Becke, N. E. Edgecombe, *J. Chem. Phys.* **1990**, *92*, 5397.
[31] A. Savin, R. Nesper, S. Wengert, T. Fässler, *Angew. Chem.* **1997**, *109*, 1892; *Angew. Chem. Int. Ed. Engl.* **1997**, *36*, 1808.
[32] S. Alvarez, „Tables of Parameters for Extended Hückel Calculations“, Universitat de Barcelona, **1989**.
[33] Different Slater exponents had already been proposed for Si-s and Si-p with $\xi_{3s} = 1.588$, $\xi_{3p} = 1.256$: P. Pyykkö, L. Lohr, *Inorg. Chem.* **1981**, *20*, 1950.
[34] E. A. Brinkman, S. Berger, J. I. Braumann, *J. Am. Chem. Soc.* **1994**, *116*, 8304.
[35] M. Elfström, *Acta Chem. Scand.* **1965**, *19*, 1694.
[36] H. L. Skriver, *The LMTO Method*, Springer, Heidelberg, **1984**.
[37] J. Burdett, *Molecular shapes; Theoretical Models of Inorganic Stereochemistry*, Wiley-Interscience, New York, **1980**.
[38] T. Albright, J. Burdett, M. Wangbo, *Orbital Interaction in Chemistry*, Wiley-Interscience, New York, **1984**.
[39] R. Dovesi, V. R. Saunders, C. Roetti, CRYSTAL92: An ab-initio Hartree-Fock LCAO programm for periodic systems, **1993**.
[40] G. M. Sheldrick, SHELXS, Göttingen, **1985** and SHELXL-96, Göttingen, **1996**.
[41] M.-H. Wangbo, M. Evain, T. Hughbanks, M. Kertesz, S. Wijeyesekera, C. Wilker, C. Zheng, R. Hoffmann, Program EHMACC: Extended Hückel Molecular and Crystal Calculations.

Received: November 23, 1998
Revised version: May 20, 1999 [F1456]